High-pulse-energy III-V-on-silicon-nitride mode-locked laser

Cite as: APL Photonics **6**, 096102 (2021); https://doi.org/10.1063/5.0058022
Submitted: 26 May 2021 • Accepted: 20 August 2021 • Published Online: 01 September 2021

Artur Hermans, Kasper Van Gasse, Jon Ø. Kjellman, et al.

High-pulse-energy III-V-on-silicon-nitride mode-locked laser

Cite as: APL Photon. 6, 096102 (2021); doi: 10.1063/5.0058022
Submitted: 26 May 2021 • Accepted: 20 August 2021 •
Published Online: 1 September 2021

Artur Hermans,[1,2,a] Kasper Van Gasse,[1,2] Jon Ø. Kjellman,[3] Charles Caër,[3] Tasuku Nakamura,[4] Yasuhisa Inada,[4] Kazuya Hisada,[4] Taku Hirasawa,[4] Stijn Cuyvers,[1,2] Sulakshna Kumari,[1,2] Aleksandrs Marinins,[3] Roelof Jansen,[3] Günther Roelkens,[1,2] Philippe Soussan,[3] Xavier Rottenberg,[3] and Bart Kuyken[1,2]

AFFILIATIONS

[1]Photonics Research Group, Department of Information Technology, Ghent University - imec, Technologiepark-Zwijnaarde 126, 9052 Ghent, Belgium
[2]Center for Nano- and Biophotonics (NB-Photonics), Ghent University, Technologiepark-Zwijnaarde 126, 9052 Ghent, Belgium
[3]imec, Kapeldreef 75, 3001 Leuven, Belgium
[4]Technology Division, Panasonic Corporation, 1006 Kadoma, Kadoma City, Osaka 571-8508, Japan

[a]**Author to whom correspondence should be addressed:** artur.hermans@ugent.be

ABSTRACT

Mode-locked lasers find their use in a large number of applications, for instance, in spectroscopic sensing, distance measurements, and optical communication. To enable widespread use of mode-locked lasers, their on-chip integration is desired. In recent years, there have been multiple demonstrations of monolithic III-V and heterogeneous III-V-on-silicon mode-locked lasers. However, the pulse energy, noise performance, and stability of these mode-locked lasers are limited by the relatively high linear and nonlinear waveguide loss, and the high temperature sensitivity of said platforms. Here, we demonstrate a heterogeneous III-V-on-silicon-nitride (III-V-on-SiN) electrically pumped mode-locked laser. SiN's low waveguide loss, negligible two-photon absorption at telecom wavelengths, and small thermo-optic coefficient enable low-noise mode-locked lasers with high pulse energies and excellent temperature stability. Our mode-locked laser emits at a wavelength of 1.6 μm, has a pulse repetition rate of 3 GHz, a high on-chip pulse energy of ≈2 pJ, a narrow RF linewidth of 400 Hz, and an optical linewidth <1 MHz. The SiN photonic circuits are fabricated on 200 mm silicon wafers in a CMOS pilot line and include an amorphous silicon waveguide layer for efficient coupling from the SiN to the III-V waveguide. The III-V integration is done by micro-transfer-printing, a technique that enables the transfer of thin-film devices in a massively parallel manner on a wafer scale.

I. INTRODUCTION

Mode-locked lasers are extremely versatile tools that can be used for distance measurements, spectroscopy, telecommunication, and astronomical spectrograph calibration, among others.[1–6] In many of these applications, bulky and expensive solid-state or fiber lasers are still the go-to solutions. On-chip integration offers the prospect of miniaturized, robust, and low-cost mode-locked laser sources. Electrically pumped, on-chip mode-locked lasers have been demonstrated in heterogeneous III-V-on-silicon and monolithic III-V technology.[7,8] A promising approach to realize low-noise, narrow-linewidth mode-locked lasers relies on the use of on-chip passive extended waveguide cavities. Both silicon and III-V passive extended cavities have been used for this purpose.[7,9] The use of long extended cavities also allows for the realization of on-chip mode-locked lasers with relatively low pulse repetition rates (repetition rates down to 1 GHz have been demonstrated[10]), a desirable feature for high-resolution spectroscopy[3] and distance metrology with a large non-ambiguity range.[11] Yet, these on-chip extended-cavity mode-locked lasers typically have pulse energies limited to several 100 fJ and RF linewidths >1 kHz.[7,12] In addition, their large temperature sensitivity makes stabilization challenging (e.g., for spectroscopy or ranging).[13]

Silicon nitride (SiN) photonic integrated circuit (PIC) technology has matured tremendously in recent years and can now be considered as one of the main photonic integration platforms,

next to the established Si and InP platforms.[14] As SiN features very low waveguide loss compared to Si and InP, it makes an excellent material for the realization of narrow-linewidth, low-noise extended-cavity lasers.[15,16] SiN PIC technology also offers the enticing prospect of low-cost, mass manufacturing using the CMOS fabrication infrastructure. In addition, SiN has a thermo-optic coefficient, which is one order of magnitude smaller than that of Si and InP,[14,17] making it less sensitive to temperature fluctuations. Moreover, SiN features negligible two-photon absorption at telecom wavelengths, which is especially important for mode-locked lasers (compared to CW lasers) as their pulsed nature gives rise to relatively high intensities.[18] Recently, a Q-switched mode-locked SiN-based laser emitting at 1.9 μm has been reported (Q-switching rate of 720 kHz, mode-locking rate of 1.2 GHz), with a thulium-doped Al_2O_3 cladding as gain medium and a Kerr-nonlinearity-based artificial saturable absorber.[19] Yet, this device still relied on an off-chip optical pump.

In this work, we demonstrate an on-chip, electrically pumped III-V-on-SiN mode-locked laser with pJ-level pulse energy, sub-kHz RF linewidth, and low temperature sensitivity. The mode-locked laser emits at a wavelength of 1.6 μm and has a low repetition rate of 3 GHz. The laser is realized by the heterogeneous integration of a III-V amplifier and saturable absorber on a low-loss SiN PIC, fabricated in a CMOS pilot line. The III-V integration is done by micro-transfer-printing, a technique that enables the transfer of thin-film devices in a massively parallel manner on a wafer scale.[20] Our results represent first steps toward high-pulse-energy, low-noise, mass-manufacturable on-chip mode-locked lasers, which we envision to be used for ranging and remote sensing. In addition, these mode-locked lasers may serve as on-chip sources for resonant supercontinuum generation in low-loss SiN cavities.[21]

II. DESIGN

Figure 1(a) shows a schematic figure of the mode-locked laser. The laser consists of a low-loss, passive SiN cavity into which the active III-V material is integrated. The active device section consists of a saturable absorber surrounded by two gain sections

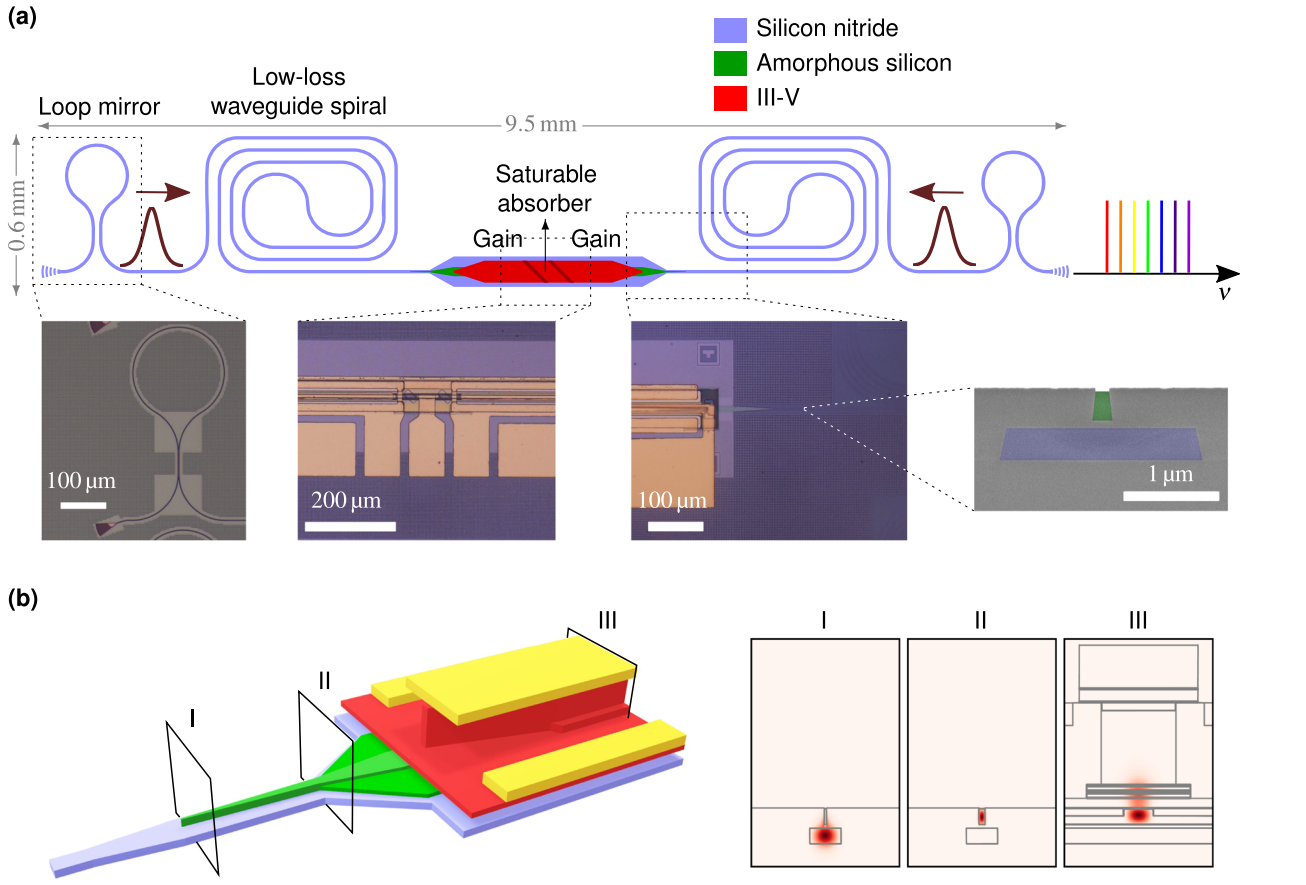

FIG. 1. (a) Schematic figure of the Fabry–Pérot colliding-pulse mode-locked laser with optical microscope images and a colored scanning electron microscope image of a waveguide cross section. The laser consists of a low-loss passive SiN (blue) cavity into which the active III-V material (red) is integrated. To get a low-loss transition from the passive SiN waveguide section to the active section, an intermediate amorphous silicon (green) waveguide layer is used. (b) Schematic illustration of the transition from the passive to the active device section, along with the simulated mode profiles (normalized electric field intensities) at several positions for a wavelength of 1610 nm. The SiN waveguide is shown in blue, the amorphous silicon waveguide in green, the III-V material in red, and the metal electrodes in yellow.

(all made out of the same III-V material). The saturable absorber is placed in the middle of the cavity, resulting in colliding-pulse mode-locking.[12] This means that there are two pulses propagating inside the cavity, which meet or collide, in the saturable absorber [as illustrated in Fig. 1(a)]. The long, low-loss SiN cavity allows us to get low repetition rates and achieve narrow linewidths. The device has a Fabry–Pérot-type architecture with loop mirrors, based on directional couplers, on each side of the cavity, allowing part of the light to be coupled out of the laser. Grating couplers are used for chip-to-fiber coupling. The grating couplers are designed for reduced back-reflections,[22] as these can render the laser unstable.

To achieve a low-loss, low-reflection transition from the low-index passive SiN section to the high-index active III-V section, we use an intermediate amorphous silicon (a-Si) waveguide layer, as illustrated in Fig. 1(b). The concept of an intermediate Si waveguide layer has been demonstrated for III-V-on-SiN amplifiers and CW lasers.[16,23] Waveguide tapers in the SiN, a-Si, and III-V layers are used to adiabatically couple light from the fundamental TE SiN waveguide mode to the fundamental TE hybrid a-Si/III-V waveguide mode.

The SiN and a-Si layers have a thicknesses of 395 and 400 nm, respectively, with 100 nm SiO_2 in between. Two etch depths are used in the a-Si layer, a full etch in the a-Si taper tip and a 180 nm shallow etch in the second part of the a-Si taper and in the hybrid a-Si/III-V section. The shallow etch allows for better heat spreading and has lower loss compared to a full-etch a-Si waveguide. The full-etch a-Si taper tips have a design width of 150 nm, which is slowly tapered to a width of 400 nm (over a length of 60 μm). Afterward, the a-Si waveguide is tapered (over a length of 80 μm) to a shallow-etch waveguide with a rib width of 2 μm. We measure a loss of 0.4 dB for a SiN-to-Si transition (at a wavelength of 1610 nm). This loss is coming mostly from the mode mismatch at the a-Si taper tip and can be lowered to <0.1 dB by improving the process parameters for narrower tip widths with near-vertical sidewalls. The measured waveguide loss for the shallow-etch a-Si waveguides is 1 dB/cm at a wavelength of 1610 nm. In the long spirals, a SiN waveguide width of 1.1 μm is used, giving a simulated dispersion parameter D_λ of ~−500 ps/(nm km) (normal dispersion). The SiN waveguides have bend radii of 100 μm. A SiN waveguide loss of 0.16 dB/cm and a bend loss below 0.01 dB/(90° bend) have been measured at a wavelength of 1610 nm. The directional couplers in the loop mirrors have waveguide widths of 850 nm and a gap between the coupled waveguides of 850 nm. The coupling lengths are 50.8 and 27.8 μm for the left and right mirror, respectively. The mirrors have a measured transmission of ~50% and 2% at a wavelength of 1610 nm. The 50% transmissive mirror serves as the output coupler of the laser. In the choice of output coupler transmission, there is a trade-off to be made: a lower transmission results not only in a lower threshold current, but also a decreased slope efficiency. 50% transmission for the output coupler is a typical number used in III-V-on-Si lasers.[12,24]

The micro-transfer-printed III-V device consists of an active multi-quantum-well (MQW) layer (six quantum wells of InAlGaAs) in between an n-type bottom slab and a p-type top cladding, similar to the III-V material used in our previous demonstrations of III-V-on-SiN amplifiers[23] and III-V-on-Si amplifiers.[25] The InAlGaAs quantum wells have a photoluminescence (PL) peak wavelength of 1520 nm. The composition of the quantum wells can be altered to change the PL peak wavelength and thereby also the emission wavelength of the mode-locked laser. As illustrated in Fig. 1(b), the MQW layer and the p-type cladding are tapered from a width below 600 nm to a width of 7 μm for the MQW layer, and 5 μm for the p-type cladding (with a taper length of 190 μm). The MQW layer is chosen to be wider than the p-type cladding to minimize the interaction between the optical mode and the sidewalls.[26] The III-V taper has a length of 190 μm, ensuring a low-loss transition and high tolerance to possible misalignment of the micro-transfer-printed III-V device.[20] The resulting mode profile in the hybrid a-Si/III-V waveguide can be seen in Fig. 1(b) (cross section III). This mode has a simulated confinement factor of 3.4% in the quantum wells (0.6% per quantum well). We opted for a relatively low confinement factor to get high pulse energies, as low confinement factors in amplifiers are known to result in large saturation powers.[25] The confinement factor in the quantum wells can easily be adjusted by changing the a-Si rib waveguide width. The III-V device consists of three electrically isolated sections: a forward bias is applied to the two outer gain sections and a reverse bias to the saturable absorber in the middle (so it acts as a photodetector). The gain sections are 1.2 mm long, and the saturable absorber is 60 μm long. The gain sections were made sufficiently long (using our previous results on amplifiers as design guidelines[23,25]) such that the gain can balance out the loss in the cavity and lasing can be achieved. The saturable absorber was chosen to be as short as could be reliably fabricated (very short saturable absorbers can give rise to open circuits in the final metallization step). For III-V-on-Si mode-locked lasers, a decrease in saturable absorber length has been demonstrated to give rise to shorter pulses.[12]

The Fabry–Pérot cavity has a total length of 48.3 mm (including the gain sections and saturable absorber), resulting in a repetition rate of 3 GHz for colliding-pulse mode-locking (two times the fundamental repetition rate since there are two pulses propagating inside the cavity). The III-V-on-SiN mode-locked laser has a total footprint of 9.5 × 0.6 mm^2.

III. FABRICATION

The heterogeneous integration of the III-V device on the SiN PIC is done through micro-transfer-printing. Micro-transfer-printing entails the process of picking up micrometer- to millimeter-sized thin-film devices from a source substrate using an elastomer stamp and printing these devices on a target substrate.[20] This transfer can be done in a massively parallel fashion on a wafer scale with submicrometer alignment accuracy. The transfer of over 10 000 devices in one printing cycle (taking less than a minute) has already been demonstrated with transfer yields of over 99.9%.[27] For the largest part of the process flow, the III-V devices and SiN PICs are processed separately on their native substrates (InP wafer for the III-V devices and silicon wafer for the SiN PICs). Therefore, established high-yield fabrication processes can be used for both the III-V and SiN processing. Only at the very end, the III-V thin-film devices are transferred to the SiN PICs with a limited amount of post-processing. As the III-V devices can be packed very densely on their native substrate, very little of the expensive III-V material goes to waste compared to the more traditional wafer bonding technology. An added advantage of micro-transfer-printing is the ease, by which devices made out of different materials—light sources, modulators,

and detectors—can be integrated on the same chip. This is especially interesting for SiN PIC technology, where active functionality is lacking.

A succinct overview of the process flow for the III-V-on-SiN mode-locked laser fabrication is shown in Fig. 2. The initial III-V epitaxial layer stack is shown in Fig. 2(a). The layer stack is as follows (from top to bottom): a 200 nm thick p-type InGaAs contact layer, a 1900 nm p-type InP layer, a 25 nm InGaAsP etch stop layer, a 40 nm InAlGaAs transition layer, a 75 nm InAlGaAs separate confinement heterostructure (SCH) layer, an InAlGaAs MQW layer, a 75 nm InAlGaAs SCH layer, a 40 nm InAlGaAs transition layer, a 230 nm n-type InP layer, a 50 nm InGaAs sacrificial layer, a 500 nm AlInAs sacrificial layer, and finally, an InP substrate. The MQW layer consists of six quantum wells of 6 nm thickness surrounded by 10 nm barriers. Figure 2(b) shows the processed III-V devices on their native substrate and a device that has been picked up for micro-transfer-printing. The sacrificial layers have been etched to create free-standing devices that are only attached to the substrate by SiN anchors. As the devices are picked up by the elastomer stamp, these anchors break in the designated spots. The III-V processing steps are similar to those described in Ref. 25 with the added step of saturable absorber definition before the p-contact definition, as Ref. 25 describes the fabrication of amplifiers, not mode-locked lasers. The saturable absorber is defined by etching 12 μm wide trenches through the *p*-InGaAs layer and ~200 nm deep into the p-InP cladding. The trenches have an angle of 45° with respect to the propagation direction to avoid possible back-reflections. Other notable differences with Ref. 25 are that we use SiN anchors instead of photoresist anchors and we define the vias before micro-transfer-printing. Defining the vias before transfer limits the amount of processing required after printing. SiN anchors are preferred over photoresist anchors in an industrial setting, as they are considered to be more stable for long-term storage (on the order of months). Figure 2(c) illustrates the printing of the III-V device on the processed SiN PIC. The PICs are processed on 200 mm wafers in imec's CMOS pilot line. The low-loss SiN waveguides are fabricated using low-pressure chemical vapor deposition (LPCVD) and deep ultraviolet lithography (wavelength of 193 nm). The essential processing steps are summarized in Fig. 1 of the supplementary material. Special mitigation techniques are used for stress and bow management of the wafers after high temperature annealing of the SiN thin film. Amorphous silicon waveguides are patterned on top of the SiN waveguides with a high aspect ratio dry etch. After oxide refill, the top surface of the 200 mm wafers is planarized by chemical-mechanical polishing (CMP) and the SiN hard mask is removed by wet etching. Before micro-transfer-printing, a 20 nm thin bisbenzocyclobutene (BCB) layer is spin coated on the PIC to ensure good adhesion of the printed III-V device. After printing, the protective resist encapsulation of the III-V device is removed in an O_2 plasma, the BCB layer is cured, and metal contact pads (40 nm Ti/1000 nm Au; Ti for better Au adhesion) are defined to probe the device [see Fig. 2(d)].

IV. CHARACTERIZATION AND DISCUSSION

For the characterization of the mode-locked laser, the chip is placed on a temperature-controlled stage that is set to a temperature of 16 °C (unless stated otherwise). The characterization setup is schematically depicted in Fig. 3(a). We use a power-ground-signal-ground-power (PGSGP) probe with a 100 μm pitch to probe the mode-locked laser electrically. The results shown here are for light collected from the left output grating coupler (at the 50% transmissive outcoupling mirror), where the highest output power is detected. The light is collected using a cleaved standard single-mode optical fiber.

Figure 3(b) shows the average optical power collected in the fiber as a function of the total gain current and the saturable absorber reverse bias. To analyze the mode-locking behavior of the laser, the emitted light is sent to a high-speed photodetector with a transimpedance amplifier (Discovery DSC-R409) whose electrical output is connected to an electrical spectrum analyzer (Keysight EXA N9010A). The measured electrical spectrum for a gain current of 295 mA and a saturable absorber bias of −2.5 V is shown in Fig. 3(c). We observe a clear signal at 2.97 GHz (with a signal-to-noise ratio of 50 dB) and its harmonics, indicating mode-locking. Figure 3(d) shows the RF power of the peak signal in a 200 MHz band centered at 3 GHz measured as a function of gain current and saturable absorber bias. We measure a large and relatively constant signal for gain currents in between 200 and 350 mA, and saturable absorber biases in between −2.5 and −2.0 V, indicating mode-locking over this wide range of bias conditions [area highlighted with a red, dotted box

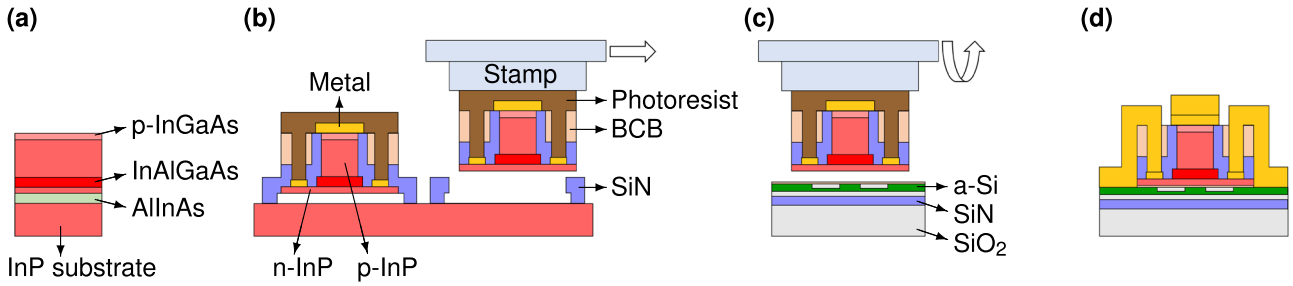

FIG. 2. Schematic device cross sections in different steps of the process flow. (a) Initial III-V epitaxial layer stack. (b) Processed III-V devices on the source InP substrate. A device has been picked up by the elastomer stamp for transfer to the target substrate. (c) Micro-transfer-printing of the III-V device on the target SiN/a-Si chip. (d) Finished laser after the final metallization step.

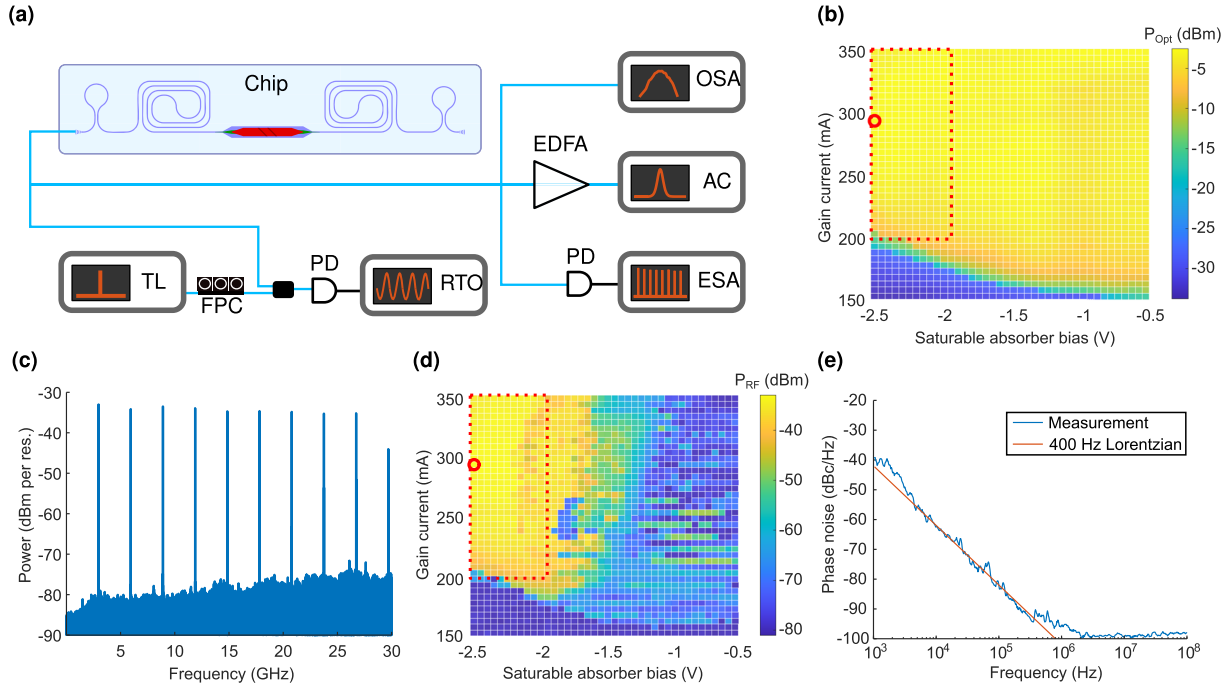

FIG. 3. (a) Schematic overview of the measurement setup. TL: tunable laser, FPC: fiber polarization controller, PD: photodetector, RTO: real-time oscilloscope, OSA: optical spectrum analyzer, EDFA: erbium-doped fiber amplifier, AC: autocorrelator, ESA: electrical spectrum analyzer. (b) Fiber-coupled optical power as a function of gain current and saturable absorber bias. (c) Electrical spectrum generated by the mode-locked laser for a gain current of 295 mA and a saturable absorber bias of −2.5 V. (d) Power of the RF signal at the repetition frequency for different gain currents and saturable absorber biases. (e) Single-sideband phase noise of the RF signal at the repetition frequency for a gain current of 295 mA and a saturable absorber bias of −2.5 V. The blue line corresponds to the measurement data and the red line to a Lorentzian function with a linewidth of 400 Hz.

in Figs. 3(b) and 3(d)]. This feature enables turnkey operation of the mode-locked laser.

For the following measurements, the mode-locked laser is biased at a fixed gain current of 295 mA (voltage of 2.5 V) and a saturable absorber voltage of −2.5 V (current of −5 mA), as the laser showed high optical power and a strong, narrow-linewidth RF signal for these bias conditions. The data points corresponding to these bias conditions are indicated with a red circle in Figs. 3(b) and 3(d). The measured average optical power in the fiber is −2.5 dBm, corresponding to an on-chip pulse energy of ~2 pJ (the measured grating coupler efficiency is −10 dB). This is significantly higher than the typical pulse energies reported for III-V-on-Si and monolithic InP-based extended-cavity mode-locked lasers.[7] Still, ≈1 pJ pulses and a 1.7 kHz RF linewidth have been reported for a III-V-on-Si extended-cavity mode-locked laser with a 4.8 GHz repetition rate (fabricated by adhesive bonding).[28] We believe the nonlinear loss in Si and InP at a wavelength of 1.6 μm is a strongly limiting factor in the pursuit of high on-chip pulse energies. This nonlinear loss is absent in SiN.[14] The pulse propagation simulations in the supplementary material show the detrimental impact of two-photon absorption and the associated free-carrier absorption. Note that even in our III-V-on-SiN mode-locked laser, there is two-photon absorption in the a-Si/III-V section that cannot readily be avoided. However, this section is very short and the effective mode area is large (≈2 μm^2), limiting the effect. We expect that pulse energies >2 pJ can be attained in III-V-on-SiN mode-locked lasers by implementing a better heat sink, increasing the saturation power of the III-V section, and decreasing the waveguide losses. Better heat dissipation can be achieved by using metallic vias connecting the III-V section with the silicon substrate, micro-transfer-printing the III-V device directly on the silicon substrate and edge coupling the light into a SiN waveguide, or gluing a heat sink on top of the fabricated laser.[29]

The RF linewidth of the peak at 2.97 GHz is determined in a single-sideband phase noise (SSB-PN) measurement.[30] The SSB-PN is measured using the direct spectrum method on a Keysight MXA ESA and the resulting SSB-PN is shown in Fig. 3(e). The measurement data match closely with a Lorentzian lineshape with a 400 Hz linewidth. The baseline at ~−100 dBc/Hz for offset frequencies over 1 MHz corresponds to the noise floor of the electrical spectrum analyzer. Our III-V-on-SiN mode-locked laser outperforms the majority of monolithic III-V and III-V-on-Si mode-locked lasers in terms of the RF linewidth.[7,12] A comparable RF linewidth of 450 Hz has been reported for a III-V-on-Si mode-locked laser with a 1 GHz repetition rate,[7,10] yet with a limited pulse energy of 0.5 pJ. An RF linewidth of 400 Hz has also been reported for an epitaxially grown quantum-dot-on-silicon laser with a 9.4 GHz repetition rate emitting at a wavelength of 1.3 μm.[8] However, its pulse energy is only 0.07 pJ and the laser is not coupled with a passive

integrated waveguide circuit, which limits the design possibilities (e.g., for the integration of dual-comb mode-locked laser systems with on-chip beam splitters/combiners, heaters, photodetectors, etc.). In the future embodiments of III-V-on-SiN mode-locked lasers, the RF phase noise and linewidth can be lowered even further by decreasing the cavity loss and increasing the cavity length.[31] While our current device has a SiN waveguide loss of 0.16 dB/cm, SiN waveguide losses below 0.001 dB/cm have been reported for low-confinement waveguides,[32] and losses as low as 0.03[33] and 0.01 dB/cm[34] for wafer-scale fabricated thick, high-confinement waveguides. The use of thick SiN waveguides with anomalous group-velocity dispersion[34] also offers exciting prospects, such as the exploration of soliton and stretched-pulse mode-locked lasers.[35]

Recording the output of the mode-locked laser with a photodetector and a real-time oscilloscope gives a clear pulse train without satellite pulses or other artifacts, indicating stable mode-locking [see Fig. 4(a)]. A DC-coupled photodetector (Discovery DSC2-30S) is used to rule out a DC signal background. As the pulse duration cannot be resolved due to the limited analog bandwidth of both the photodetector and real-time oscilloscope, an intensity autocorrelation measurement is performed. The intensity autocorrelation measurement is done with the pulseCheck optical autocorrelator from APE GmbH. The pulses emitted by the mode-locked laser are amplified by an L-band EDFA before being sent to the autocorrelator, as intensity autocorrelation measurements require relatively high peak powers. The autocorrelation trace is shown in Fig. 4(b) and corresponds to a pulse duration of 8 ps assuming a sech^2 pulse shape. Note that sending the pulses through an EDFA can cause significant pulse distortion.[36] Our simulations (in which we numerically solve a Ginzburg–Landau-type equation as described in Ref. 37) indicate that there is a ≈2.5 ps difference in pulse duration between the output and input of the EDFA. Advanced stepped-heterodyne measurements that do not require pulse amplification have been suggested to determine the pulse envelope for semiconductor mode-locked lasers.[38] Sub-ps pulses have been demonstrated for III-V-on-Si and monolithic InP-based mode-locked lasers with repetition rates ≥20 GHz and pulse energies limited to ≈0.1 pJ.[7] Pulse durations tend to go up for lower repetition rates.[12] Regardless, pulse durations on the order of 10 ps have been shown to be sufficient for high-resolution spectroscopy.[39] For the observed 3 dB optical bandwidth of 2 nm [see Fig. 5(a)], a minimum pulse duration of

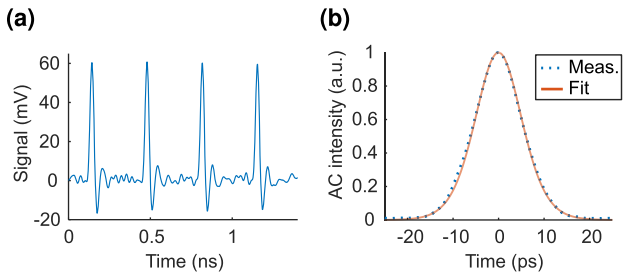

FIG. 4. (a) Pulse train of the mode-locked laser recorded by a 160 GS/s real-time oscilloscope. (b) Intensity autocorrelation measurement of the emitted pulses amplified by an L-band EDFA.

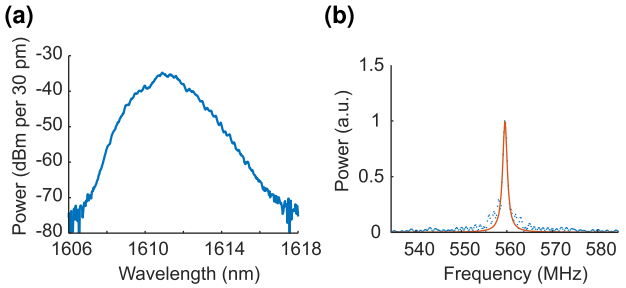

FIG. 5. (a) The optical spectrum. The optical power, expressed in dBm, is shown per 30 pm wavelength range (which is the resolution of the optical spectrum analyzer). (b) Measurement of the optical linewidth by heterodyning one of the laser lines near the center of the spectrum with a stable, narrow-linewidth reference laser (Santec TSL-770, linewidth 60 kHz). The measurement data (blue) are fitted with a Lorentzian function (red).

1.4 ps can be expected (a transform-limited sech^2 pulse has a time-bandwidth product of 0.315).[35] The transform-limited pulse shape can also be calculated directly from the measured optical spectrum, yielding a pulse duration of 1.3 ps. On-chip dispersive elements can be used to get closer to this pulse duration.[40–42] With its pJ-level pulse energy and ps pulse duration, our III-V-on-SiN mode-locked laser shows great promise for on-chip spectral broadening through resonant supercontinuum generation: in a recent demonstration, a broad comb was generated by pumping a SiN microresonator with pulses of 1–6 pJ in energy and >1 ps in duration (supplied by an off-chip source).[21]

The optical spectrum of the mode-locked laser is shown in Fig. 5(a). The spectrum was measured using an optical spectrum analyzer (Anritsu MS9740A) with a resolution of 30 pm, which is too low to resolve the individual laser lines. We observe a 10 dB bandwidth of over 4 nm corresponding to more than 154 lines. There is a small amount of ripple on the optical spectrum, which is likely due to the presence of spurious reflections in the laser cavity, possibly caused by the passive-to-active device transitions. We expect this can be improved upon in the future devices by altering the process conditions and transition design. The optical linewidth is measured by beating a line in the center of the spectrum with a narrow-linewidth reference laser (Santec TSL-770, linewidth 60 kHz) on a high-speed photodetector. The resulting signal is recorded with a Keysight real-time oscilloscope and post-processed in MATLAB. By taking the fast Fourier transform (FFT) of a 1 μs time trace, the heterodyne beat note linewidth can be determined. The result is shown in Fig. 5(b). The peak of the RF signal lies at ≈560 MHz, which corresponds to the optical frequency difference between the laser line and the reference laser. Fitting the measurement data with a Lorentzian function yield a narrow optical linewidth of ~1 MHz. However, it is important to note that the simulated instrumental lineshape also has a 1 MHz linewidth. Therefore, the value of 1 MHz should be considered an upper bound for the optical linewidth. Optical linewidths of 29, 10.6, and 0.3 MHz have been reported for a 30 GHz monolithic InP-based mode-locked laser,[43] a 20 GHz quantum-dot-on-Si mode-locked laser,[4] and a 1 GHz III-V-on-Si mode-locked laser,[10] respectively. A decrease in cavity loss and/or an increase in cavity length is expected to lead to lower optical linewidths.[44] The linewidth can also be

reduced by using a fast saturable absorber or active mode-locking.[44] A fast on-chip saturable absorber could for instance be achieved by means of a Kerr-based artificial saturable absorber.[19] $LiNbO_3$-[45] or lead-zirconate-titanate-based[46] on-chip high-speed modulators could be used for active mode-locking. Although we do not measure the carrier-envelope offset frequency (e.g., by f-to-$2f$ self-referencing),[47] our measurements are consistent with the generation of a comb.

The temperature sensitivity of the mode-locked laser is measured by recording the time-averaged beat note frequency between a laser line and a narrow-linewidth reference laser for varying temperatures of the temperature-controlled stage. The measured resulting shift in the beat note frequency is shown in Fig. 6(a). Fitting gives a frequency shift of 3 MHz/mK. This matches well with the estimated shift assuming a thermo-optic coefficient of 2.45×10^{-5} K^{-1} for SiN,[14] $\frac{\Delta\nu}{\Delta T} \approx \frac{dn}{dT}\frac{\nu}{n} \approx 2.3$ MHz/mK. Finally, we record the beat note frequency fluctuations over a time interval of 30 s, while the temperature-controlled stage is set to a fixed temperature of 16 °C [see Fig. 6(b)]. We envisage our on-chip mode-locked lasers to be used for ranging and spectroscopic sensing. These applications typically only require millisecond acquisition times, much shorter than the 30 s interval shown here, to measure a distance or an absorption spectrum.[39,48] The beat note frequency fluctuates over an interval of ~80 MHz wide, which corresponds to temperature fluctuations of 27 mK. This is the best temperature stability we could achieve without the use of a temperature-controlled container and the chip being influenced by ambient conditions. For III-V-on-Si and monolithic InP-based mode-locked lasers, the temperature-induced frequency fluctuations are expected to be an order of magnitude larger, in accordance to their thermo-optic coefficients.[14,17]

The above discussion focused on device characterization and fabrication- and design-related suggestions for improved device performance. To demonstrate the potential of III-V-on-SiN mode-locked lasers in applications, dedicated system-level experiments will have to be conducted. Stabilization of the mode-locked laser(s) typically leads to improved system performance.[47] Yet, also simple, free-running mode-locked lasers can be sufficiently stable for certain applications, as demonstrated for dual-comb ranging,[48] dual-comb spectroscopy,[49] and optical communication.[4] Our III-V-on-SiN mode-locked laser could be stabilized by locking a laser line to an ultrastable reference laser through an optical phase-locked loop[2] (using on-chip phase shifters) or optical injection locking.[24] Hybrid-mode locking can be used to lock the repetition rate of the mode-locked laser to a stable RF synthesizer.[24] Dual-comb-based applications could benefit from the integration of two mode-locked lasers on a single chip, in close proximity to each other, to ensure a high level of mutual stability.[49]

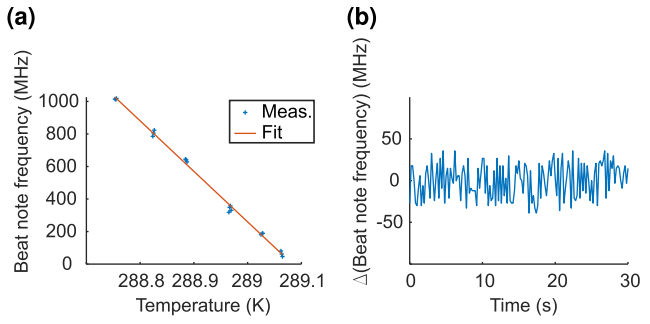

FIG. 6. (a) Measurement of beat note frequency between a line in the center of the laser spectrum and a narrow-linewidth reference laser as a function of temperature. For each data point, we average over a time of 30 s. The measurement data (blue) are fitted with a line (red). (b) Measurement of the beat note frequency fluctuations over a time interval of 30 s while the temperature-controlled stage is set to a fixed temperature of 16 °C.

V. CONCLUSION

We have demonstrated an on-chip, electrically pumped III-V-on-SiN mode-locked laser with a small line spacing of 3 GHz, emitting at a wavelength of 1.6 μm. With a pulse energy of ≈2 pJ, RF linewidth of 400 Hz, low temperature sensitivity, and the use of scalable fabrication techniques, this demonstration opens the road toward the realization of high-performance, compact, low-cost mode-locked lasers as desired for laser ranging and remote sensing, among others. The availability of low-loss, dispersion-engineered SiN cavities also opens up exciting possibilities for on-chip spectral broadening and novel mode-locked laser designs.

SUPPLEMENTARY MATERIAL

See the supplementary material for an overview of the SiN PIC fabrication and pulse propagation simulations.

ACKNOWLEDGMENTS

We thank S. Poelman, S. Verstuyft, J. Zhang, C. Op de Beeck, S. Uvin, J. Goyvaerts, and B. Haq for the useful discussions on device design and III-V processing.

Portions of this work were presented at the Conference on Lasers and Electro-Optics 2021.[50]

DATA AVAILABILITY

The data that support the findings of this study are available from the corresponding author upon reasonable request.

REFERENCES

[1] K. Minoshima and H. Matsumoto, "High-accuracy measurement of 240-m distance in an optical tunnel by use of a compact femtosecond laser," Appl. Opt. **39**, 5512–5517 (2000).

[2] I. Coddington, W. C. Swann, L. Nenadovic, and N. R. Newbury, "Rapid and precise absolute distance measurements at long range," Nat. Photonics **3**, 351–356 (2009).

[3] N. Picqué and T. W. Hänsch, "Frequency comb spectroscopy," Nat. Photonics **13**, 146–157 (2019).

[4] S. Liu, X. Wu, D. Jung, J. C. Norman, M. J. Kennedy, H. K. Tsang, A. C. Gossard, and J. E. Bowers, "High-channel-count 20 GHz passively mode-locked quantum dot laser directly grown on Si with 4.1 Tbit/s transmission capacity," Optica **6**, 128–134 (2019).

[5] S. Koenig, D. Lopez-Diaz, J. Antes, F. Boes, R. Henneberger, A. Leuther, A. Tessmann, R. Schmogrow, D. Hillerkuss, R. Palmer, T. Zwick, C. Koos, W. Freude, O. Ambacher, J. Leuthold, and I. Kallfass, "Wireless sub-THz communication system with high data rate," Nat. Photonics **7**, 977–981 (2013).

[6] T. Steinmetz, T. Wilken, C. Araujo-Hauck, R. Holzwarth, T. W. Hänsch, L. Pasquini, A. Manescau, S. D'Odorico, M. T. Murphy, T. Kentischer, W. Schmidt,

and T. Udem, "Laser frequency combs for astronomical observations," Science **321**, 1335–1337 (2008).
[7]K. Van Gasse, S. Uvin, V. Moskalenko, S. Latkowski, G. Roelkens, E. Bente, and B. Kuyken, "Recent advances in the photonic integration of mode-locked laser diodes," IEEE Photonics Technol. Lett. **31**, 1870–1873 (2019).
[8]D. Auth, S. Liu, J. Norman, J. E. Bowers, and S. Breuer, "Passively mode-locked semiconductor quantum dot on silicon laser with 400 Hz RF line width," Opt. Express **27**, 27256–27266 (2019).
[9]V. Moskalenko, K. A. Williams, and E. A. J. M. Bente, "Pulse narrowing and RF linewidth reduction of integrated passively mode-locked laser in anticolliding design by means of spectral tuning," IEEE Photonics J. **8**, 1502810 (2016).
[10]Z. Wang, K. Van Gasse, V. Moskalenko, S. Latkowski, E. Bente, B. Kuyken, and G. Roelkens, "A III-V-on-Si ultra-dense comb laser," Light: Sci. Appl. **6**, e16260 (2017).
[11]P. Trocha, M. Karpov, D. Ganin, M. H. P. Pfeiffer, A. Kordts, S. Wolf, J. Krockenberger, P. Marin-Palomo, C. Weimann, S. Randel, W. Freude, T. J. Kippenberg, and C. Koos, "Ultrafast optical ranging using microresonator soliton frequency combs," Science **359**, 887–891 (2018).
[12]M. L. Davenport, S. Liu, and J. E. Bowers, "Integrated heterogeneous silicon/III-V mode-locked lasers," Photonics Res. **6**, 468–478 (2018).
[13]K. Van Gasse, J. Huh, Z. Chen, S. Poelman, Z. Wang, G. Roelkens, T. W. Hänsch, B. Kuyken, and N. Picqué, "III-V-on-silicon mode-locked laser with 1-GHz line spacing for dual-comb spectroscopy," in *Conference on Lasers and Electro-Optics* (Optical Society of America, 2020), p. SF1G.5.
[14]A. Rahim, E. Ryckeboer, A. Z. Subramanian, S. Clemmen, B. Kuyken, A. Dhakal, A. Raza, A. Hermans, M. Muneeb, S. Dhoore, Y. Li, U. Dave, P. Bienstman, N. Le Thomas, G. Roelkens, D. Van Thourhout, P. Helin, S. Severi, X. Rottenberg, and R. Baets, "Expanding the silicon photonics portfolio with silicon nitride photonic integrated circuits," J. Lightwave Technol. **35**, 639–649 (2017).
[15]K.-J. Boller, A. van Rees, Y. Fan, J. Mak, R. E. M. Lammerink, C. A. A. Franken, P. J. M. van der Slot, D. A. I. Marpaung, C. Fallnich, J. P. Epping, R. M. Oldenbeuving, D. Geskus, R. Dekker, I. Visscher, R. Grootjans, C. G. H. Roeloffzen, M. Hoekman, E. J. Klein, A. Leinse, and R. G. Heideman, "Hybrid integrated semiconductor lasers with silicon nitride feedback circuits," Photonics **7**, 4 (2020).
[16]C. Xiang, W. Jin, J. Guo, J. D. Peters, M. J. Kennedy, J. Selvidge, P. A. Morton, and J. E. Bowers, "Narrow-linewidth III-V/Si/Si_3N_4 laser using multilayer heterogeneous integration," Optica **7**, 20–21 (2020).
[17]D. Melati, A. Waqas, A. Alippi, and A. Melloni, "Wavelength and composition dependence of the thermo-optic coefficient for InGaAsP-based integrated waveguides," J. Appl. Phys. **120**, 213102 (2016).
[18]J. Mak, A. van Rees, Y. Fan, E. J. Klein, D. Geskus, P. J. M. van der Slot, and K.-J. Boller, "Linewidth narrowing via low-loss dielectric waveguide feedback circuits in hybrid integrated frequency comb lasers," Opt. Express **27**, 13307–13318 (2019).
[19]K. Shtyrkova, P. T. Callahan, N. Li, E. S. Magden, A. Ruocco, D. Vermeulen, F. X. Kärtner, M. R. Watts, and E. P. Ippen, "Integrated CMOS-compatible Q-switched mode-locked lasers at 1900 nm with an on-chip artificial saturable absorber," Opt. Express **27**, 3542–3556 (2019).
[20]J. Zhang, G. Muliuk, J. Juvert, S. Kumari, J. Goyvaerts, B. Haq, C. Op de Beeck, B. Kuyken, G. Morthier, D. Van Thourhout, R. Baets, G. Lepage, P. Verheyen, J. Van Campenhout, A. Gocalinska, J. O'Callaghan, E. Pelucchi, K. Thomas, B. Corbett, A. J. Trindade, and G. Roelkens, "III-V-on-Si photonic integrated circuits realized using micro-transfer-printing," APL Photonics **4**, 110803 (2019).
[21]M. H. Anderson, R. Bouchand, J. Liu, W. Weng, E. Obrzud, T. Herr, and T. J. Kippenberg, "Photonic chip-based resonant supercontinuum via pulse-driven Kerr microresonator solitons," Optica **8**, 771–779 (2021).
[22]J. H. Song, B. Snyder, K. Lodewijks, R. Jansen, and X. Rottenberg, "Grating coupler design for reduced back-reflections," IEEE Photonics Technol. Lett. **30**, 217–220 (2018).
[23]C. Op de Beeck, B. Haq, L. Elsinger, A. Gocalinska, E. Pelucchi, B. Corbett, G. Roelkens, and B. Kuyken, "Heterogeneous III-V on silicon nitride amplifiers and lasers via microtransfer printing," Optica **7**, 386–393 (2020).
[24]S. Uvin, S. Keyvaninia, F. Lelarge, G.-H. Duan, B. Kuyken, and G. Roelkens, "Narrow line width frequency comb source based on an injection-locked III-V-on-silicon mode-locked laser," Opt. Express **24**, 5277–5286 (2016).
[25]B. Haq, S. Kumari, K. Van Gasse, J. Zhang, A. Gocalinska, E. Pelucchi, B. Corbett, and G. Roelkens, "Micro-transfer-printed III-V-on-silicon C-band semiconductor optical amplifiers," Laser Photonics Rev. **14**, 1900364 (2020).
[26]K. Van Gasse, R. Wang, and G. Roelkens, "27 dB gain III-V-on-silicon semiconductor optical amplifier with >17 dBm output power," Opt. Express **27**, 293–302 (2019).
[27]R. S. Cok, M. Meitl, R. Rotzoll, G. Melnik, A. Fecioru, A. J. Trindade, B. Raymond, S. Bonafede, D. Gomez, T. Moore, C. Prevatte, E. Radauscher, S. Goodwin, P. Hines, and C. A. Bower, "Inorganic light-emitting diode displays using micro-transfer printing," J. Soc. Inf. Disp. **25**, 589–609 (2017).
[28]S. Keyvaninia, S. Uvin, M. Tassaert, Z. Wang, X. Fu, S. Latkowski, J. Marien, L. Thomassen, F. Lelarge, G. Duan, G. Lepage, P. Verheyen, J. Van Campenhout, E. Bente, and G. Roelkens, "III-V-on-silicon anti-colliding pulse-type mode-locked laser," Opt. Lett. **40**, 3057–3060 (2015).
[29]R. Loi, J. O'Callaghan, B. Roycroft, Z. Quan, K. Thomas, A. Gocalinska, E. Pelucchi, A. J. Trindade, C. A. Bower, and B. Corbett, "Thermal analysis of InP lasers transfer printed to silicon photonics substrates," J. Lightwave Technol. **36**, 5935–5941 (2018).
[30]F. Kéfélian, S. O'Donoghue, M. T. Todaro, J. G. McInerney, and G. Huyet, "RF linewidth in monolithic passively mode-locked semiconductor laser," IEEE Photonics Technol. Lett. **20**, 1405–1407 (2008).
[31]R. Paschotta, "Noise of mode-locked lasers (Part II): Timing jitter and other fluctuations," Appl. Phys. B **79**, 163–173 (2004).
[32]J. F. Bauters, M. J. R. Heck, D. D. John, J. S. Barton, C. M. Bruinink, A. Leinse, R. G. Heideman, D. J. Blumenthal, and J. E. Bowers, "Planar waveguides with less than 0.1 dB/m propagation loss fabricated with wafer bonding," Opt. Express **19**, 24090–24101 (2011).
[33]H. El Dirani, L. Youssef, C. Petit-Etienne, S. Kerdiles, P. Grosse, C. Monat, E. Pargon, and C. Sciancalepore, "Ultralow-loss tightly confining Si_3N_4 waveguides and high-Q microresonators," Opt. Express **27**, 30726–30740 (2019).
[34]J. Liu, G. Huang, R. N. Wang, J. He, A. S. Raja, T. Liu, N. J. Engelsen, and T. J. Kippenberg, "High-yield, wafer-scale fabrication of ultralow-loss, dispersion-engineered silicon nitride photonic circuits," Nat. Commun. **12**, 2236 (2021).
[35]A. M. Weiner, *Ultrafast Optics* (John Wiley & Sons, Inc., 2009).
[36]J. Yu, P. Jeppesen, B. Palsdottir, and S. N. Knudsen, "Reducing pulsewidth broadening in L-band EDFAs by use of a new L-band EDF," IEEE Photonics Technol. Lett. **13**, 654–656 (2001).
[37]G. P. Agrawal, "Optical pulse propagation in doped fiber amplifiers," Phys. Rev. A **44**, 7493–7501 (1991).
[38]A. Verschelde, K. Van Gasse, B. Kuyken, M. Giudici, G. Huyet, and M. Marconi, "Analysis of the phase-locking dynamics of a III-V-on-silicon frequency comb laser," OSA Continuum **4**, 129–136 (2021).
[39]Z. Chen, K. Van Gasse, E. Vicentini, J. Huh, S. Poelman, Z. Wang, G. Roelkens, T. W. Hänsch, B. Kuyken, and N. Picqué, "High-resolution dual-comb gas-phase spectroscopy with a mode-locked laser on a photonic chip," in *Conference on Lasers and Electro-Optics* (Optical Society of America, 2020), p. JTh4A.8.
[40]D. T. H. Tan, K. Ikeda, R. E. Saperstein, B. Slutsky, and Y. Fainman, "Chip-scale dispersion engineering using chirped vertical gratings," Opt. Lett. **33**, 3013–3015 (2008).
[41]D. T. H. Tan, P. C. Sun, and Y. Fainman, "Monolithic nonlinear pulse compressor on a silicon chip," Nat. Commun. **1**, 116 (2010).
[42]G. F. R. Chen, T. Wang, C. Donnelly, and D. T. H. Tan, "Second and third order dispersion generation using nonlinearly chirped silicon waveguide gratings," Opt. Express **21**, 29223–29230 (2013).
[43]J. S. Parker, A. Bhardwaj, P. R. A. Binetti, Y.-J. Hung, and L. A. Coldren, "Monolithically integrated gain-flattened ring mode-locked laser for comb-line generation," IEEE Photonics Technol. Lett. **24**, 131–133 (2012).
[44]R. Paschotta, A. Schlatter, S. C. Zeller, H. R. Telle, and U. Keller, "Optical phase noise and carrier-envelope offset noise of mode-locked lasers," Appl. Phys. B **82**, 265–273 (2006).
[45]T. Vanackere, M. Billet, C. Op de Beeck, S. Poelman, G. Roelkens, S. Clemmen, and B. Kuyken, "Micro-transfer printing of lithium niobate on silicon nitride," in *European Conference on Optical Communication* (Institute of Electrical and Electronics Engineers, 2020), p. Mo1C-5.

[46]K. Alexander, J. P. George, J. Verbist, K. Neyts, B. Kuyken, D. Van Thourhout, and J. Beeckman, "Nanophotonic Pockels modulators on a silicon nitride platform," Nat. Commun. **9**, 3444 (2018).
[47]T. Fortier and E. Baumann, "20 years of developments in optical frequency comb technology and applications," Commun. Phys. **2**, 153 (2019).
[48]T.-A. Liu, N. R. Newbury, and I. Coddington, "Sub-micron absolute distance measurements in sub-millisecond times with dual free-running femtosecond Er fiber-lasers," Opt. Express **19**, 18501–18509 (2011).
[49]P. Guay, N. B. Hébert, V. Michaud-Belleau, D. G. Lancaster, and J. Genest, "Methane spectroscopy using a free-running chip-based dual-comb laser," Opt. Lett. **44**, 4375–4378 (2019).
[50]A. Hermans, K. Van Gasse, J. Ø. Kjellman, C. Caër, T. Nakamura, Y. Inada, K. Hisada, T. Hirasawa, S. Kumari, A. Marinins, R. Jansen, G. Roelkens, P. Soussan, X. Rottenberg, and B. Kuyken, "III-V-on-silicon-nitride mode-locked laser with 2 pJ on-chip pulse energy," in *Conference on Lasers and Electro-Optics* (Optical Society of America, 2021), p. SM1A.1.